

Different P_{In} antisites in n - and p -type InP

H. J. Sun, H. P. Gislason,* C. F. Rong,[†] and G. D. Watkins
Department of Physics, Lehigh University, Bethlehem, Pennsylvania 18015
 (Received 15 July 1993)

Several P_{In} antisite structures are observed in InP and identified using optical detection of magnetic resonance (ODMR) and electron-nuclear double resonance (ODENDOR) via magnetic circular dichroism in near-band-gap absorption. One of these is the isolated P_{In} antisite previously studied in as-grown and electron-irradiated p -type InP. Two others, clearly distinguishable in the ODENDOR, are perturbed antisites that are produced by electron irradiation and observed only in n -type samples. The isolated antisite is also detected by ODMR and ODENDOR in as-grown p -type materials in two competing photoluminescence bands, peaking at 0.8–0.9 and 1.1 eV. It is proposed that both bands arise from donor-acceptor pair recombination involving the isolated antisite defect, the 0.8–0.9-eV band originating from the $P_{\text{In}}^+/P_{\text{In}}^{2+}$ donor level and the 1.1-eV band from the $P_{\text{In}}^0/P_{\text{In}}^+$ donor level. With this identification, the energy position of the isolated antisite $P_{\text{In}}^+/P_{\text{In}}^{2+}$ level is estimated to be at $E_V + 1.1 \pm 0.1$ eV and that of its $P_{\text{In}}^0/P_{\text{In}}^+$ level to be at $E_V + 1.39 \pm 0.03$ eV. The perturbed antisite levels appear higher in the gap consistent with the presence of an acceptor in a near-neighbor shell, a likely candidate being the indium vacancy.

I. INTRODUCTION

A magnetic-resonance signal attributed to the anion antisite P_{In} in InP was to our knowledge first observed by conventional electron paramagnetic resonance (EPR) (Ref. 1) and later by optically detected magnetic resonance (ODMR) via magnetic circular dichroism (MCD) in absorption,² and photoluminescence (PL).^{3,4}

Different assignments for the level position of the double P_{In} donor based on PL-ODMR measurements of Zn-doped material, both electron irradiated⁴ and as-grown,³ have been reported in the literature.^{3–6} A photoluminescence band at 0.8–0.9 eV which is enhanced at resonance was first assigned to transitions between shallow donor states and the $P_{\text{In}}^0/P_{\text{In}}^+$ level⁴, which was therefore deduced to be 0.8–0.9 eV below the conduction band. Later studies in p -type material showed that the PL band originated from transitions between the $P_{\text{In}}^+/P_{\text{In}}^{2+}$ level and shallow acceptor states.^{3,5,6} Hence, the second ionization level of the antisite was concluded to be 0.8–0.9 eV above the valence band.

The above level assignments count on the ability of the ODMR technique to distinguish between different

antisite-related complexes which produce very similar signals but can have significantly different level positions. In fact, previous investigations have suggested the existence of more than one antisite structure with differences in g values and hyperfine coupling constants close to the resolving power of the ODMR and EPR techniques when applied to all of the III-V semiconductors. In particular, slightly different g values and central hyperfine interactions have been reported in ODMR and EPR measurements for p -type Zn-doped InP, on the one hand, and n -type Sn-doped InP, on the other.^{1,7} Table I summarizes a few values from the literature.

In this report we first prove by measuring the ODENDOR (optical detection of electron-nuclear double resonance) signal of the nearest In shell that several antisite-related defects with very similar ODMR signals do indeed exist in InP. Moreover, these signals often appear simultaneously in the ODMR measurements overlapping each other. In this case level assignments based on such measurements have to be made with extreme caution.

Second, our ODENDOR measurements on as-grown p -type InP:Zn identify the antisite defect observed in PL-ODMR and the one measured in MCD as both arising from the isolated antisite.⁸ With this information and

TABLE I. Selected g values and central hyperfine coupling constants reported in the literature.

Dopant [cm ⁻³]	e -irrad. [cm ⁻²]	Conductivity after irr	g value	A_0 [10 ⁻⁴ cm ⁻¹]	Measurement
[Zn]= 1.2×10^{16}	as-grown	p	2.000 ± 0.003	980 ± 20	MCD (Ref. 8)
[Zn]= 3×10^{17}	1×10^{17}	p	2.000 ± 0.003	980 ± 20	MCD (Ref. 8)
[Zn]= $\sim 10^{16}$	as-grown	p	2.006 ± 0.005	1000 ± 20	PL (Ref. 3)
[Zn]= 5.6×10^{17}	1.3×10^{18}	p	2.012 ± 0.005	1040 ± 20	MCD (Ref. 7)
[Sn]= 2×10^{17}	2.3×10^{18}	n	1.992 ± 0.008	920 ± 50	EPR (Ref. 1)
[Sn]= 2×10^{17}	2.3×10^{18}	n	1.991 ± 0.005	990 ± 20	MCD (Ref. 7)

measurements of the emission and excitation spectra for photoluminescence and the PL-ODMR signals, we are able to present a direct estimate of the energy positions of the P_{In}^{0/+} and P_{In}^{+ /2+} levels of the P_{In} isolated antisite. Finally, we propose a tentative model for the perturbed antisites and their energy levels.

II. EXPERIMENTAL PROCEDURE

The InP crystals used in this study include different *n*- and *p*-type single crystals grown by the liquid-encapsulated Czochralski method. The as-grown samples of interest for the present paper are listed in Table II. Some of them were electron irradiated with 2.5-MeV electrons from a Van de Graaff accelerator. They were mounted on a water-cooled holder during irradiation, and care was taken to keep the sample current density low, at about 4 μA/cm². Data for the samples at selected irradiation fluences are also given in Table II. The table also summarizes *g* values and center P-hyperfine coupling constants determined from the ODMR spectra, as well as

other pertinent results which will be discussed in the following sections. The carrier type after electron irradiation was estimated from conductivity measurements on a few representative samples.⁹ From these studies, it was established that *p*-type samples convert to *n* type at a critical electron flux (in e⁻/cm²) approximately equal to the *p*-type doping concentration (in no./cm³), and that *n*-type samples remain *n* type.

All experiments were performed in an Oxford Instruments SM-4 optical cryostat with a built-in superconducting magnet and quartz windows allowing operation at pumped liquid-helium temperature (1.7 K). The sample, mounted on a quartz rod at the end of a long stainless-steel tube, was placed in a 35-GHz TE₀₁₁ microwave cavity designed in the form of concentric rings for optical access, and was immersed in the liquid helium (1.7 K) during the experiment.

For MCD experiments, the excitation source was a 600-W tungsten-halogen lamp. A Jarrel-Ash, Mark X, ¼-meter monochromator selected wavelength, and colored glass filters removed unwanted orders. A Po-

TABLE II. Summary of the experimental results on representative samples. (yes) denotes evidence of a weak signal.

Label	Dopant (cm ⁻³)	<i>e</i> -rad. (cm ⁻²)	ODMR	ODENDOR			<i>g</i> value	Hyperfine <i>A</i> (10 ⁻⁴ cm ⁻¹)
				23	26 (MHz)	165		
1B	[Zn]=5×10 ¹⁵	as-grown	MCD					
1C	[Zn]=5×10 ¹⁵	1×10 ¹⁶	MCD				1.995±0.005	940±30
1A	[Zn]=5×10 ¹⁵	3×10 ¹⁷	MCD	(yes)	yes	(yes)	1.990±0.005	940±30
2A	[Zn]=1.2×10 ¹⁶	as-grown	MCD	yes		yes	2.000±0.003	980±20
			PL	yes		yes	1.997±0.005	980±30
3A	[Zn]=3×10 ¹⁷	as-grown	PL	yes		yes	1.997±0.005	980±30
3B	[Zn]=3×10 ¹⁷	1×10 ¹⁷	MCD	yes		yes	2.000±0.003	980±20
3C	[Zn]=3×10 ¹⁷	1×10 ¹⁸	MCD	yes		yes		
4A	Semi-insu	as-grown						
4B	Semi-insu	3×10 ¹⁷	MCD	(yes)	yes	(yes)	1.990±0.005	940±30
4C	Semi-insu	1×10 ¹⁸	MCD		yes		1.990±0.005	930±30
5B	[Si]=5×10 ¹⁵	as-grown						
5A	[Si]=5×10 ¹⁵	3×10 ¹⁷	MCD	(yes)	yes	(yes)	1.990±0.005	940±30
5C	[Si]=5×10 ¹⁵	1×10 ¹⁸	MCD				1.988±0.005	940±30
6A	[Si]=1.4×10 ¹⁶	as-grown						
6B	[Si]=1.4×10 ¹⁶	2×10 ¹⁶						
6C	[Si]=1.4×10 ¹⁶	3.6×10 ¹⁷	MCD		yes		1.990±0.005	930±30
7A	[Sn]=5-9×10 ¹⁵	as-grown						
7B	[Sn]=5-9×10 ¹⁵	2×10 ¹⁶	MCD		yes		1.987±0.005	950±30
7C	[Sn]=5-9×10 ¹⁵	3.6×10 ¹⁷	MCD		yes		1.990±0.005	920±30
8A	[Sn]=1-3×10 ¹⁶	as-grown						
8B	[Sn]=1-3×10 ¹⁶	2×10 ¹⁶						
8C	[Sn]=1-3×10 ¹⁶	3.6×10 ¹⁷	MCD		yes		1.990±0.005	930±30
9A	[Sn]=3-20×10 ¹⁶	as-grown						
9B	[Sn]=3-20×10 ¹⁶	2×10 ¹⁶						
9C	[Sn]=3-20×10 ¹⁶	3.6×10 ¹⁷	MCD		yes		1.989±0.005	940±30

laroid HR linear polarizer and Hinds PEM-3 photoelastic modulator produced alternating left and right circularly polarized light at 50.4 kHz. A North Coast liquid-nitrogen-cooled Ge detector (EO-817p) collected the transmitted light propagating along the static magnetic field. The output of the detector was synchronously lock-in amplified at 50.4 KHz so that the recorded signal was proportional to the transmission difference between right- and left-circular polarizations.

MCD is defined as the difference in absorption coefficients for left (α_L) and right (α_R) circularly polarized light.⁸ When $(\alpha_L - \alpha_R)d \ll 1$ (i.e., $I_R - I_L \ll I_R + I_L$, the condition of our experiments), one obtains the simple relation

$$\text{MCD } A \equiv \alpha_L - \alpha_R \cong \frac{2}{d} \frac{I_R - I_L}{(I_R + I_L)}, \quad (1)$$

where d is the thickness of the sample, and I_R and I_L are the transmitted right and left circularly polarized components, respectively. All values given for the MCD in this paper were determined in the above manner, the lock-in signal (proportional to $I_R - I_L$) being divided by the average transmitted light. In this way, the spectral response of the light source, monochromator, detector, lenses, windows, etc., as well as unrelated absorption in the sample were automatically corrected for.

ODMR spectra were obtained by monitoring the change in MCD induced by microwave transitions between Zeeman-split components of the ground state as the magnetic field was swept. To determine the spectral dependence of an MCD-ODMR signal, two wavelength scans were performed—one with the magnetic field tuned to the resonance, another with the magnetic field shifted off—and the difference was taken. In this way, unrelated contributions to the MCD were eliminated. For the ODENDOR studies, a two-turn coil was installed in the cavity such that its magnetic-field axis was perpendicular to both the static and microwave magnetic fields. The radio frequency was supplied to the coil from a Fluke 6060B frequency synthesizer amplified by an ENI 3100LA solid-state radio-frequency amplifier. The static magnetic field was tuned to the peak of the ODMR resonance, and changes in the ODMR signal intensity were recorded as the radio frequency was swept. The frequency sweep of the synthesizer was computer controlled, and digital signal averaging was performed as necessary.

For PL studies, photoluminescence was excited by a Ti-sapphire laser and detected by a North Coast EO-817s cooled germanium detector. ODMR spectra were recorded by monitoring changes in the PL intensity synchronous with on-off amplitude modulation of the microwaves as a function of the static magnetic field. Spectral dependence studies of the PL and the PL-ODMR were performed by inserting a Jarrel-Ash, Mark X, $\frac{1}{4}$ -meter monochromator with appropriate higher-order elimination filters before the detector, and were corrected for the spectral response of the monochromator and detector. For the PL-ODMR spectral response studies, the difference between the signal on and off resonance was taken to avoid unrelated background signals. For

ODENDOR studies, the change in ODMR intensity induced by cw radio-frequency transitions was recorded on the computer as a function of radio frequency.

III. MCD STUDIES

Figure 1 shows representative MCD-ODMR spectra of three samples from Table II. The spectra were measured at ~ 910 nm (1.36 eV) in the tail of an absorption band peaking above the band gap.

They all show the characteristic doublet signature of the P_{In} antisite, but close inspection reveals differences in the central hyperfine interaction, the g value, and the linewidth of the ODMR resonance. The p -type sample no. 2 is the only as-grown sample in the figure, and is the particular sample previously studied by Jeon *et al.*,⁸ for which it was established by ODENDOR that the ODMR signal arises from the isolated antisite. Its antisite spectrum in curve *a* is centered at somewhat lower field and has a slightly greater spacing between the dips of the doublet than the remaining curves in Fig. 1. Therefore the g value and central P-hyperfine interaction A_0 deduced from the antisite spectrum of the as-grown sample no. 2 are larger than the values measured in the other samples illustrated in the figure, which are n type.

As-grown n -type samples are too lossy to allow magnetic-resonance measurements which prevents direct comparison between as-grown n - and p -type samples. A typical result, however, for n -type material electron irradiated just enough to compensate for the shallow doping is shown in Fig. 1 (curve *c*) for sample no. 5A. Further irradiation of this material does not change the g and A_0 values significantly. Sample no. 1A of Fig. 1 (curve *b*), originally p type but converted to n type through electron irradiation (see below), shows similar g and A_0 values. These results and those of many other samples are collected in Table II, where it is apparent that all the n -type and semi-insulating materials display the similar smaller g and A_0 values.

The higher resolution of ODENDOR measurements

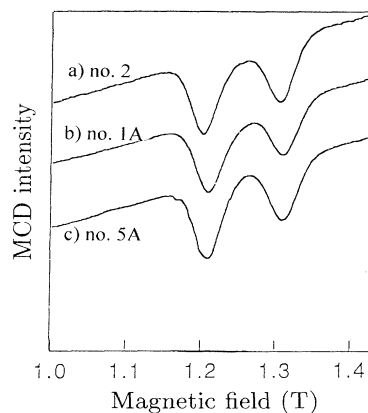


FIG. 1. MCD-ODMR spectra detected at $\lambda = 910$ nm with $\mathbf{B} \parallel [100]$ for (curve *a*) as-grown p -type sample no. 2; (curve *b*) electron-irradiated, originally p -type, sample no. 1A; and (curve *c*) electron-irradiated n -type sample no. 5A.

serves to explain the origin of these spectral differences. Figure 2 shows parts of the ODENDOR spectra for each of the three samples of Fig. 1. The spectra were taken by monitoring the characteristic P_{In} ODMR doublet in Fig. 1, with the magnetic field set to the low-field transition and $\mathbf{B} \parallel [100]$. The shift of the resonance frequency versus magnetic field B for all spectra is $+9.3 \pm 0.5$ MHz/T. This is the nuclear gyromagnetic ratio of both of the ^{113}In and ^{115}In isotopes which identifies all of the ENDOR transitions as arising from an In shell around the P_{In} antisite.

Figure 2 (curve *a*) shows the ODENDOR spectrum of the as-grown p -type sample no. 2. The signal resonance line at 23 MHz identifies it as arising from the first In shell around the isolated antisite.⁸ The corresponding nearest-neighbor ^{31}P lines at ~ 165 MHz which were analyzed in Ref. 8 are also present in the ODENDOR spectrum but not shown in the figure.

Electron irradiation of lightly doped p -type materials, which converts them to n type, produces an entirely different second-neighbor In shell ODENDOR spectrum, revealing therefore a perturbed antisite structure. The spectrum is characterized by two prominent peaks at about 24 and 27 MHz, and is clearly distinguishable from the one in the Fig. 2 (curve *a*). The angular dependence of these partially resolved lines is very complex. Attempts to analyze it have been unsuccessful so far, but suggest low symmetry. Figure 2 (curve *b*) shows the ODENDOR signal of sample no. 1A produced by e irradiation of the p -type material no. 1 to a fluence of 3×10^{17} cm^{-2} (converted to n type). At 165 MHz weak ^{31}P lines of the isolated antisite are observed in this sample. The intensity of these lines is not correlated to the In lines at 24 and 27 MHz, however.

Hence we conclude that the In lines at 23 MHz of the isolated antisite are also present in the spectrum of Fig. 2 (curve *b*) but buried in the strong new resonances. Figure 2 (curve *c*) shows the same spectral region for sample no. 5A of Fig. 1 (curve *c*) which is an n -type sample, electron

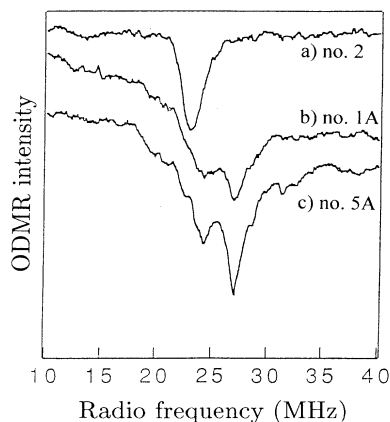


FIG. 2. ODENDOR spectra with $\mathbf{B} \parallel [100]$ for the samples of Fig. 1 in the same order. The spectra were measured with the magnetic field tuned to the low-field ODMR transition.

irradiated to just compensate for the shallow donors. The ODENDOR signals are very similar to those of sample no. 1A in Fig. 2 (curve *b*). Again, weak P lines at 165 MHz, not shown in the figure, give evidence for the presence also of the isolated antisite in this sample. The corresponding 23-MHz In lines are not resolved. Further irradiation of the n -type material no. 5 broadens and changes the relative intensities of the two new peaks, indicating that they each arise from different antisite-related defects. We label them $P_{In}X$ (24-MHz peak) and $P_{In}Y$ (27-MHz peak), the X and Y denoting a nearby perturbing impurity or other defect.

Figure 3 shows the spectral dependences of the ODMR signals of three samples in which different antisite spectra dominate as determined by ODENDOR. In Fig. 3 (curve *a*), the spectral dependence of the ODMR signal is shown for the as-grown sample no. 2, where the isolated antisite was identified. Figure 3 (curve *b*) presents the spectral dependence of the ODMR signal measured in sample no. 1A, in which the $P_{In}X$ and $P_{In}Y$ defects dominate. This sample has been electron irradiated to 3×10^{17} cm^{-2} .

It has been established for the isolated antisite that the peak of the MCD absorption band is above the band gap, only the low-energy tail of the band being seen.⁸ The spectral dependence of the perturbed antisites appears to be similar. Therefore these two types of antisites cannot easily be distinguished from the spectral dependence of their MCD alone. In Fig. 3 (curve *c*), we also include the MCD-ODMR spectral dependence of a heavily doped (3×10^{17} cm^{-3}) p -type sample no. 3 C which has been heavily irradiated ($\phi = 1 \times 10^{18}$ cm^{-2}). As shown in Table II, this sample displays only the isolated antisite, but its spectral dependence appears substantially different from that of no. 2 in Fig. 3 (curve *a*). We will return to a possible explanation for this later in Sec. V.

Table II summarizes the ODMR and ODENDOR re-

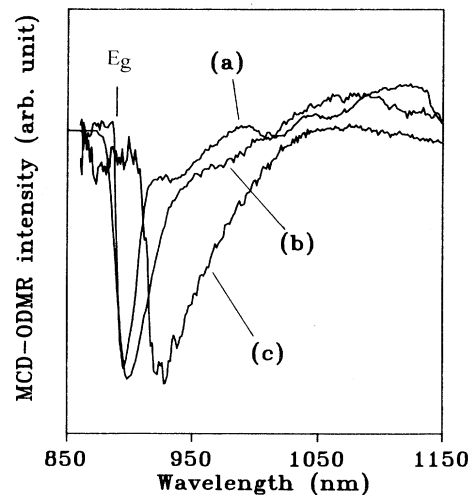


FIG. 3. Spectral dependence of the MCD-ODMR signal for three samples: (curve *a*) as-grown p -type sample no. 2; (curve *b*) e -irradiated sample no. 1A; and (curve *c*) e -irradiated sample no. 3C.

sults for the samples listed. From this we can conclude that for the isolated antisite, $g = 2.000 \pm 0.003$, and $A_0 = 980 \pm 30 \times 10^{-4} \text{ cm}^{-1}$. For the perturbed antisites, $g = 1.990 \pm 0.005$, and $A_0 = 940 \pm 30 \times 10^{-4} \text{ cm}^{-1}$.

In an earlier study,¹⁰ we demonstrated in more detail that the spectral shape and relative strength of the 24- and 27-MHz peaks in the complicated ODENDOR signal are not constant, and depend not only upon the irradiation dose, but also the wavelength, and additional side illumination which serves to alter charge states of defects. This supplies further evidence that these two peaks arise from different perturbed antisites. In that earlier publication, we also reported a careful study of the emergence of the MCD and MCD-ODMR of the perturbed antisites in n -type materials vs electron irradiation fluence. From this study, it was concluded that the perturbed antisites are not initially present in the as-grown material, but are produced instead by the electron irradiation (as opposed to being initially present but revealed by the irradiation-produced change in the Fermi-level position). Further, the presence of the 24- and 27-MHz lines in all of the differently doped, electron-irradiated materials of Table II reveals that the dopant atoms are not part of the perturbed antisites.

In the MCD-ODMR studies of the isolated antisite,⁸ strong anisotropic ODENDOR signals were found in the 140–200-MHz range arising from the four nearest-neighbor phosphorus atoms. (The lines collapse into a single set at ~ 165 MHz for $\mathbf{B} \parallel [100]$, the conditions of our measurements described here.) No corresponding lines have been detected in this region for the perturbed antisites. We now explore the reasons for this failure: In addition to differences in the g values and central hyperfine interaction constants A_0 , the linewidth of the ODMR transitions is slightly larger for the $P_{\text{In}}X$ and $P_{\text{In}}Y$ antisite defects than for the isolated one. Since the linewidth represents unresolved hyperfine interactions with neighboring In and P shells averaged over the unpaired electron wave function of the defect, this difference may be used to make a rough estimate of the frequency position expected for the P ODENDOR lines of the perturbed antisites. In the following, for simplicity, we treat $P_{\text{In}}X$ and $P_{\text{In}}Y$ as a single defect.

The $S = \frac{1}{2}$ spin Hamiltonian describing the ODMR spectrum of the P antisite can be written as

$$H = g\mu_B \mathbf{S} \cdot \mathbf{B} + A_0 \mathbf{I}_0 \cdot \mathbf{S} + \sum_i \mathbf{I}_i \cdot \tilde{A}_i \cdot \mathbf{S}, \quad (2)$$

where the first term describes the Zeeman interaction of the electronic spin with the external field \mathbf{B} , the second term the hyperfine interaction with the central P atom, and the last term the interaction with nuclei on neighboring atomic sites. For the $\Delta M_S = \pm 1$ ODMR transitions, accurate to first order in $A_0/g\mu_B B$, $A_i/g\mu_B B$, this gives

$$B = \frac{1}{g\mu_B} \left[h\nu - A_0 m_0 - \sum_i A_i m_i \right], \quad (3)$$

where ν is the microwave frequency (35 GHz), m_0 and m_i are the azimuthal quantum numbers for the central P nu-

cleus, and the i th-neighbor nuclei, respectively, and

$$A_i = |\hat{\xi} \cdot \tilde{A}_i|, \quad (4)$$

where $\hat{\xi}$ is a unit vector along \mathbf{B} .

Adding to Eq. (2) the Zeeman interaction of the nuclei with the central field B , the $\Delta m_i = \pm 1$ ENDOR transitions for the neighboring i nuclei become, to the same order of approximation,

$$\nu_i = \frac{1}{h} \left| A_i M_S - \frac{\mu_i}{I_i} B \right|, \quad (5)$$

where μ_i is the magnetic moment, and I_i the nuclear spin of the i th nucleus. Since μ_i is known to be positive for ^{113,115}In and ³¹P, A_0 and A_i must be positive. This in turn reveals that the ENDOR transitions are being observed in the $M_S = -\frac{1}{2}$ state, the observed frequencies being larger than $\mu_i B / I_i h$ in each case. The ODENDOR measurements were made with $\mathbf{B} \parallel [100]$, and tuned to the low-field $m_0 = +\frac{1}{2}$ transition at 1.8 T (Fig. 1). With Eq. (5), the transitions at 23 and 165 MHz for the isolated antisite therefore correspond to $A_{\text{In}}/h = +23$ MHz, and $A_P/h = +285$ MHz. The average position of the In lines for the combined perturbed antisite structure (Fig. 2, curves b and c) around 26 MHz corresponds to $\langle A_{\text{In}} \rangle / h \sim +29$ MHz.

Equation (3) describes the $m_0 = \pm \frac{1}{2}$ resolved central hyperfine splitting observed in the ODMR spectrum, as well as the broadening of the two lines that arises from unresolved hyperfine interactions with the remaining neighbors contained in the last term. We now show that this last term can be used to provide a rough estimate of an average nearest-neighbor P value $\langle A_P/h \rangle$ for the new antisite structures.

If the nearest-neighbor P shell is intact for both antisites, the combination of four equivalent P atoms would

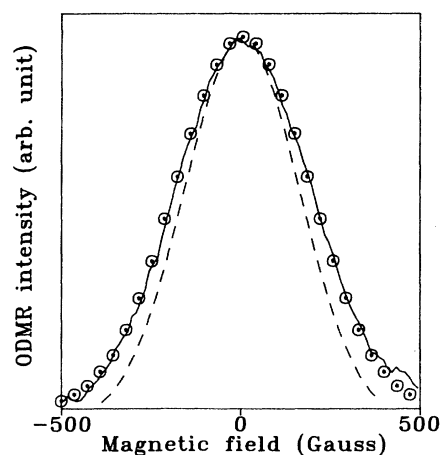


FIG. 4. Simulated line shapes for the isolated antisite (dashed curve, using $A_P/h = 285$ MHz and $A_{\text{In}}/h = 23$ MHz) and the perturbed antisite (circled points, using $\langle A_P \rangle/h = 360$ MHz and $\langle A_{\text{In}} \rangle/h = 29$ MHz). The solid curve gives the experimental result for the perturbed antisite measured in electron-irradiated sample no. 8C.

TABLE III. Summary of values characterizing the antisite defects in the study.

Defect	g value	A_0 [10^{-4} cm $^{-1}$]	$\frac{\langle A_{In} \rangle}{h}$ [MHz]	$\frac{\langle A_P \rangle}{h}$ [MHz]	W [G]
P_{In}	2.000	980±20	23	285	340±15
P_{InX}, P_{InY}	1.990	940±30	29	~360	410±15

give five ODMR lines with intensity ratio 1:4:6:4:1 for **B** in the [100] direction. We assume that each of these lines is in turn broadened primarily through interaction with the 12 $I = \frac{9}{2}$ In nuclei in the second-neighbor shell. Using the values $A_{In}/h = 23$ MHz, and $A_P/h = 285$ MHz, a good fit is found to the full width at half maximum (FWHM) linewidth of 340 ± 15 G, which matches with the value measured for the isolated antisite in the as-grown p -type sample no. 2. The dashed curve in Fig. 4 shows the simulated line shape.

Next we insert the larger value of $\langle A_{In} \rangle/h = 29$ MHz and use $\langle A_P \rangle/h$ as a fitting parameter to obtain the FWHM linewidth of the ODMR transitions of the perturbed antisites, 410 ± 30 G. In order to account for this linewidth, we arrive at $\langle A_P \rangle/h = 360$ MHz, which gives the circled points in Fig. 4. The figure also includes the experimental line shape for a typical n -type sample (solid line). The value obtained for $\langle A_P \rangle/h$ corresponds to ENDOR transitions around 200 MHz under the above conditions. Close inspection indeed reveals faint structure around 200 MHz, which appears to show a μ/Ih field shift close to that of P. However, the lines at present are far too weak to study their angular variation and extract the symmetry information that they contain. [There are several reasons that can account for their weakness. In the first place, there are at least two perturbed defects, each with reduced symmetry, so that their four phosphorus neighbors are no longer equivalent and the intensity is divided therefore between several components. Second, our efficiency in getting higher radio-frequency magnetic fields into the cavity is believed to be greatly reduced, due either to the geometry of our rf coil in the cavity or to exceeding the stated range (180 MHz) of the ENI 3100LA amplifier. Evidence for this is found in the angular dependence of the isolated antisite,⁸ where the intensity was found to drop dramatically above ~ 200 MHz.] Table III summarizes these values for the isolated and perturbed antisite structures.

IV. PHOTOLUMINESCENCE

Figure 5(a) shows the PL spectrum of the as-grown p -type sample no. 2 ($[Zn] = 1.2 \times 10^{16}$ cm $^{-3}$) when excited at 1.405 eV (obtained by a tunable Ti-sapphire laser), which is just slightly below the band gap (1.424 eV). The spectrum appears to consist of two photoluminescence bands. One band has a peak around 0.9 eV. Another band has a relatively weaker peak around 1.1 eV. Both bands are broad and overlap each other. The identical but more intense photoluminescence bands are observed in the more heavily doped p -type, as-grown sample no. 3.

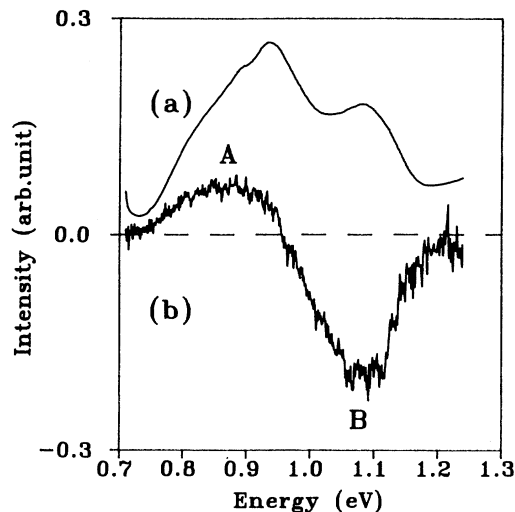


FIG. 5. Emission spectral dependence of as-grown p -type sample no. 2: (a) PL; (b) PL-ODMR. The excitation energy was 1.405 eV, the modulation frequency 500 Hz.

In both samples these luminescence bands are rapidly quenched by electron irradiation.

When monitoring the PL in either sample, a strong PL-ODMR antisite signal is detected. In Fig. 5(b), the spectral dependence of the PL-ODMR signal detected at 500-Hz (microwave on-off) modulation frequency is presented. The spectral dependence of the PL-ODMR signal differs from the PL spectrum in several respects. First, a positive PL-ODMR signal peaks at ~ 0.88 eV, lower in energy than the peak in the PL at ~ 0.93 eV. We label the ~ 0.88 eV antisite-related band as band *A*. Second, a negative ODMR peak, labeled *B*, is present at ~ 1.1 eV, close to the position of the weaker PL band but with strength greater than *A*. Third, and more importantly, the ODMR resonance arising from the *A* luminescence band increases the PL intensity (the change of the PL is positive), whereas the ODMR resonance arising from the *B* band decreases the PL intensity (the change of the PL is negative).

Figure 6 shows the ODMR spectra which correspond to the different emission bands shown in Fig. 5(b). A monochromator has been inserted in front of the detector, so that the *A* and *B* bands are monitored separately. The spectra are taken at a microwave modulation frequency of 12 Hz. Figure 6(a) presents the ODMR spectrum when monitoring the *A* band. The microwave-induced change in the photoluminescence shows the characteristic two-peak antisite spectrum and gives a positive increase in luminescence. Each peak has a FWHM of about 350 G. The spectrum is still detectable as the modulation frequency is increased to 5 KHz. The best signal to noise ratio is obtained with an excitation power density between 0.05 and 0.3 W/cm 2 . The signals are saturated when the excitation power density exceeds 0.3 W/cm 2 . Figure 6(b) presents the ODMR signals when monitoring the *B* band. The microwave-induced change causes a decrease in the luminescence. The ODMR sig-

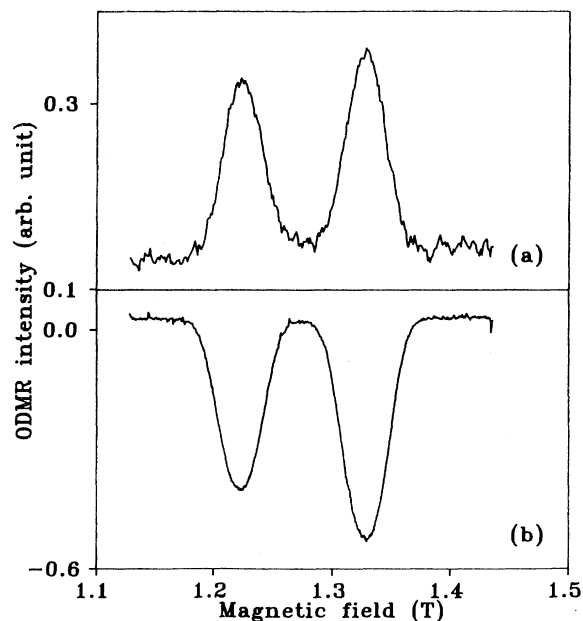


FIG. 6. ODMR spectra of the antisite at 12-Hz modulation frequency. (a) Detected in the *A* band (FWHM of ~ 350 G). (b) Detected in the *B* band (FWHM of ~ 500 G).

nal of the *B* band displays a somewhat flatter top with a FWHM of about 500 G. The best signal to noise is obtained with an excitation power density between 0.01 and 0.04 W/cm². The signals are saturated rapidly when the excitation power density exceeds 0.04 W/cm². The signals decrease rapidly when the excitation power density exceeds 0.04 W/cm². The signals decrease rapidly as the modulation frequency is increased, the signals becoming very weak and difficult to detect beyond ~ 500 Hz. The ODMR line shape and linewidth seen in each band are independent of the microwave power, and affected only slightly by the power of the excitation. The position of the ODMR signal for each is unchanged, and the *g* and *A*₀ values appear characteristic of the isolated antisite.

The relative strength of the two PL-ODMR signals, observed in these two bands, depends greatly upon the excitation energy and the modulation frequency of microwaves. One of the important observations is that PL-ODMR is detected simultaneously in both *A* and *B* bands only with the excitation wavelength within the narrow range from 890 to 872 nm (1.39–1.42 eV). This is demonstrated in Fig. 7, which presents the spectral dependence of the antisite PL-ODMR signal under different excitation wavelengths for sample no. 2, obtained in the same way as for Fig. 5(b), with the exception that the microwave modulation frequency is now 12 Hz. Figure 7(a) was detected with 890-nm excitation (~ 1.39 eV), and the spectrum is dominated by the PL-ODMR band *A*. There is only a very weak sign of the PL-ODMR band *B*. In Fig. 7(b), the excitation wavelength is 882 nm (~ 1.40 eV). Here the relative strength of the two ODMR bands has changed dramatically, the spec-

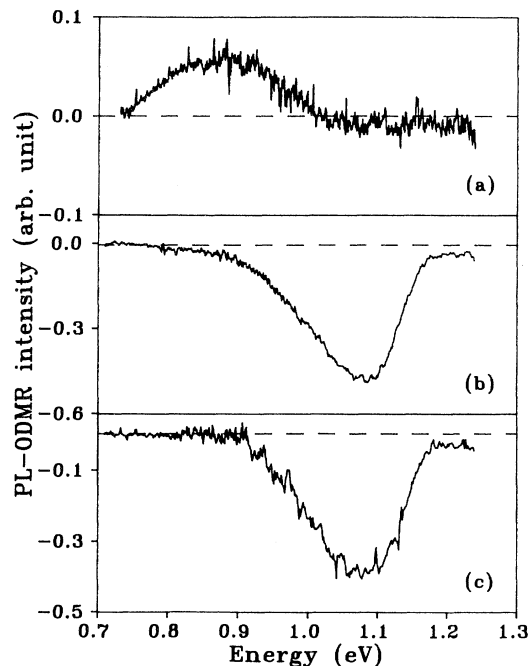


FIG. 7. Spectral dependence of the antisite PL-ODMR signal with modulation frequency of 12 Hz: (a) $\lambda_{\text{ex}} = 890$ nm (1.39 eV); (b) $\lambda_{\text{ex}} = 882$ nm (1.41 eV); (c) $\lambda_{\text{ex}} = 866$ nm (1.43 eV), slightly higher than the band gap (1.424 eV).

trum being dominated by the *B* band. [Note that in Fig. 5(b), with the identical excitation condition, the *A* band is more prominent. This reflects the effects of the modulation frequency, which in that case was 500 Hz.] Figure 7(c) gives the spectral dependence of the PL-ODMR signals with 866 nm (~ 1.43 eV) excitation, slightly higher than the InP band gap.

PL-ODENDOR was performed to examine the possibility that different antisite defects give rise to the different PL-ODMR and MCD-ODMR signals. The results are presented in Fig. 8, in which the ODENDOR signal of the In shell was monitored. All spectra were detected in the as-grown sample no. 2. In both the MCD and PL cases, the magnetic field was tuned to the low-field ODMR resonance. Figure 8 (curve *a*) presents the ODENDOR signal of the In shell, but monitoring the MCD absorption at 910 nm. Figure 8 (curve *b*) presents the ODENDOR signal, but detecting it in the 0.88 eV PL-ODMR *A* band shown in Fig. 5(b). Figure 8 (curve *c*) presents the ODENDOR signal, but detecting it in the 1.10 eV PL-ODMR *B* band. The PL-ODENDOR signals shown in Fig. 8, curves *b* and *c* are identical with curve *a*, which was previously shown to represent the undistorted nearest-neighbor In shell of the isolated antisite.⁸ The PL-ODENDOR measurements reveal therefore that the PL-ODMR signals arising from both the *A* and *B* PL-ODMR bands arise from the *isolated antisite*.

In the case of the more heavily doped as-grown *p*-type sample no. 3, again the ODMR spectra for the *A* and *B* bands show similar characteristics to sample no. 2, and

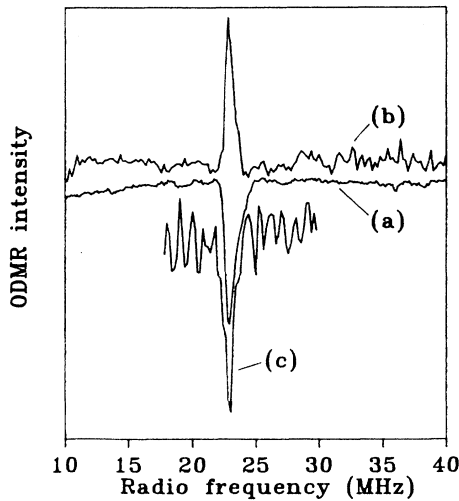


FIG. 8. In-shell ODENDOR spectra for as-grown sample no. 2, with the magnetic field tuned to the low-field ODMR resonance: (curve *a*) MCD at 910 nm; (curve *b*) 0.8–0.9 eV PL-ODMR band; and (curve *c*) 1.1 eV PL-ODMR band.

the PL-ODENDOR reveals the isolated antisite. However, the PL-ODMR strength of the *B* band is much weaker than that of sample no. 2. (The 165-MHz nearest-neighbor phosphorous signals are also present in the *A* spectrum, but are absent in the *B* spectrum.) This proves the remarkable fact that the paramagnetic state of the isolated antisite is indeed observed both in absorption and in two separate PL-ODMR bands in the as-grown *p*-type sample no. 2. This is not the case for the more heavily doped *p*-type sample no. 3, for which PL-ODENDOR reveals the isolated antisite, but MCD-ODMR is absent. In the lightly doped as-grown *p*-type sample no. 1, PL-ODMR is absent.

Figure 9 gives the excitation spectral dependence of the PL-ODMR signals of the isolated antisite for sample no. 2, while monitoring the total PL (*A* + *B* bands). The excitation source was a Ti-sapphire tunable laser pumped by an argon-ion laser. Low excitation power was used in order to avoid saturation of the PL-ODMR signals, and the PL-ODMR signal intensity was normalized to a constant excitation power.

Figure 9(a) was taken at microwave modulation frequency of 1.1 KHz. From the study of the emission spectral dependence of the PL-ODMR signal shown in Figs. 5(b) and 7, we know that Fig. 9(a) is related to the ODMR spectrum *A* shown in Fig. 6(a). The spectrum shows a strong excitation peak near the band-gap region, but also significant excitation in the 1.24–1.38-eV range. The 1.24-eV excitation is the limit of our titanium-sapphire tunable laser. Extrapolation of the data indicates an excitation threshold to observe the ODMR spectrum *A* at ~ 1.20 eV. (The decrease in the strength of the PL-ODMR signals when the excitation energy exceeds the band gap presumably reflects the reduced penetration of the light.) Figure 9(b) was detected at a microwave modulation frequency of 12 Hz. Again, the

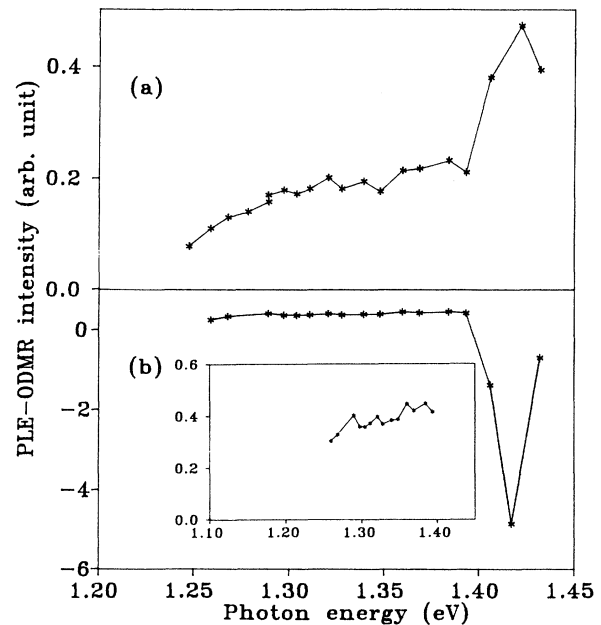


FIG. 9. Excitation spectral dependence of the PL-ODMR signals for sample no. 2: (a) 1.1 KHz modulation; (b) 12-Hz modulation, with inset at higher gain in the 1.26–1.39-eV region.

spectrum shows a strong excitation peak near the band-gap region, but in this case it is negative (decrease in PL). A weak but measurable positive excitation in the 1.24–1.38-eV range is also observed. Figure 9(b) therefore consists of two contributions. One contribution is related to ODMR spectrum *A*, which makes a positive increase in the PL. However, when the excitation energy exceeds 1.39 eV, another contribution arising from ODMR spectrum *B*, as shown in Fig. 6(b), starts to dominate and obscure the contribution from *A*. On the other hand, ODMR spectrum *B* is not detectable at the 1.1-KHz modulation frequency of Fig. 6(a). It is evident that ODMR spectrum *B* arises from an efficient recombination center, which competes strongly with that giving rise to ODMR spectrum *A*. The microwave-induced transition causes a strong decrease in the *B* PL. The excitation threshold to detect ODMR spectrum *B* is accurately estimated to be $\sim 1.39 \pm 0.01$ eV. Shown with expanded vertical gain in the inset of Fig. 9(b) is the excitation spectrum of the positive *A* ODMR signal. It is clear here, at 12-Hz modulation, that the excitation threshold has shifted to lower energies than that (~ 1.2 eV) estimated in Fig. 9(a) for 1.1-KHz modulation.

Figure 10 presents the emission spectral dependence of the PL-ODMR signals at two different excitation energies; (a) 1.34 and (b) 1.39 eV, for modulation frequency at (I) 1.1 KHz and (II) 12 Hz. These excitation energies are below the threshold for the *B* luminescence (see Fig. 9), and the curves therefore reflect the *A* spectral dependence. The solid curves, indicated within the spectra, result from Gaussian smoothing. Two features are observed in the figure: (1) for a given excitation, as the

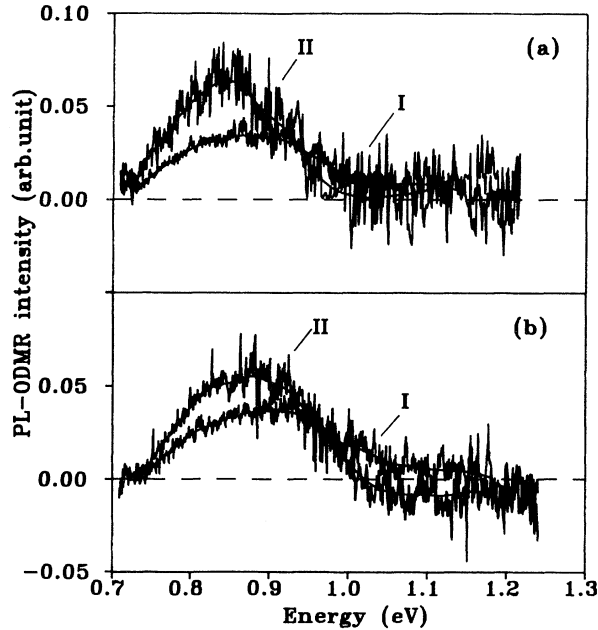


FIG. 10. Spectral dependence of the PL-ODMR at two different excitation energies below the threshold for B PL: (a) 1.34 and (b) 1.39 eV, for modulation frequencies at (I) 1.1 KHz and (II) 12 Hz.

modulation frequency is decreased, the peak position of the A band shifts to lower energies; (2) at a fixed modulation frequency, the peak position of the A band shifts to higher energies with an increase in the excitation energy. The maximum shift of the peak position is ~ 0.1 eV. [The high-energy onsets of the curves also indicate a shift in the same sense as expected vs modulation frequency and excitation. However, the apparent onset could be affected by a small negative contribution from the PL-ODMR band B —particularly evident in curve II of Fig. 10(b)—and is therefore less accurate. There is no significant contribution from B near the A peak, and the peak determination should be reliable].

As described earlier in this section, the width of each of the B -band PL-ODMR lines, Fig. 6(b), is significantly greater than that observed in the A band or by MCD-ODMR (500 vs 350 G). This is unexpected, since we have established that all three arise from the isolated P_{In}^+ antisite. To explain this, we suggest that the radiative lifetime of the recombination process plays a major role. As described earlier in this section, ODMR spectrum B is strongest at low modulation frequencies. It has been established in previous studies^{3,12} that the modulation frequency for maximum ODMR signal, ω_m , can be a direct measure of the lifetime of the rate-limiting process of the photoluminescence, with $\tau \sim 1/\omega_m$. Therefore, this result reveals a significantly longer lifetime in either the excited radiative state for B , or in some intermediate state involved in the generation process for it, as compared to A .

In general, the linewidth of an EPR transition is broadened primarily from unresolved hyperfine interac-

tions (inhomogeneous broadening), as discussed in Sec. III. In the usual case, the lifetime in the radiative paramagnetic state is shorter than that of nuclear-spin relaxation. Under the microwave resonance condition, therefore, the ODMR resonance saturates only a specific spin packet of the inhomogeneously broadened line (which is the envelope of all such packets), “burning a hole.” The specific spin packet represents one particular value of the local field to which many nuclei contribute. In the case of the isolated antisite, the major source of line broadening arises from hyperfine interaction between the electron and the four equivalent $I = \frac{1}{2}$ phosphorus nearest neighbors, which gives five unresolved ODMR lines with intensity ratio 1:4:6:4:1 for $\mathbf{B} \parallel [001]$. Each of these lines is broadened in turn through interactions between the electron and the 12 $I = \frac{3}{2}$ In next-nearest neighbors. This is the case calculated successfully in Sec. III for the MCD-ODMR spectra.

However, if the lifetime in the excited P_{In}^+ paramagnetic state is long enough to be comparable with or longer than that of nuclear-spin relaxation, the absorbed microwave energy is not confined to a specific spin packet, but can spread out to other packets as the nuclei flip and change the local field seen by each defect. This energy “diffusion” tends to equalize the intensity ratio for the five unresolved ODMR lines, producing a broader flat-topped line, because saturation of all can be accomplished by tuning to any of them. There is a consequent increase in the ODMR intensity, and a corresponding decrease in the ODENDOR intensity. This explains the B spectrum in Fig. 6(b), where the linewidth and shape of the ODMR transitions have changed in this fashion. Also, as demonstrated in Fig. 9, the strength of ODMR spectrum B is ~ 10 times larger than that of ODMR spectrum A , but the strength of the In ODENDOR signal of the 1.1 eV B band remains comparable to that of the In ODENDOR signal of the 0.88-eV B band. At the same time, the 165-MHz nearest-neighbor phosphorus signals are absent in the B band. This is evidence that all spin packets separated by the nearest-neighbor P spin flips are saturated under the electron-spin resonance for band B , and it is the near-neighbor phosphorus nuclear relaxation that is short enough to be comparable to the P_{In}^+ lifetime.

V. DISCUSSION

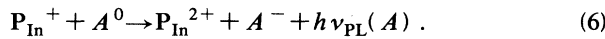
A. Model for the photoluminescence

1. A band

The P_{In} antisite, as a double donor, introduces two energy levels in the band gap, $P_{\text{In}}^+/P_{\text{In}}^{2+}$ and $P_{\text{In}}^0/P_{\text{In}}^+$. Previous studies have detected antisite-related PL-ODMR only in the A photoluminescence band peaking at 0.8–0.9 eV.^{3–6} In these studies, consistent with the results described here, the resonance was reported to be strong in as-grown Zn-doped samples with hole concentration in the range 10^{15} – 10^{16} cm^{-3} .³ A P_{In}^+ PL-ODMR resonance has also been reported in as-grown samples with hole concentrations as high as 5.6×10^{17}

cm^{-3} .⁵ When electron irradiated to a fluence of $3 \times 10^{17} \text{ cm}^{-2}$, such samples still showed the ODMR resonance in PL.^{4,6} The same samples did not exhibit MCD-ODMR in the as-grown condition, but a detection onset at an irradiation dose of $3 \times 10^{16} \text{ cm}^{-2}$ was reported.^{4,6} Consequently, for e -irradiation fluences between 3×10^{16} and $3 \times 10^{17} \text{ cm}^{-2}$ these samples showed a P_{In}^+ resonance both in emission (PL) and absorption (MCD). The reported PL-ODMR signal was weak, however, and the possibility of the two antisite resonances being different was not addressed in the early literature.

Since the isolated antisite P_{In}^+ is an electron-spin- $\frac{1}{2}$ defect, we conclude that the origin of the A band is donor-acceptor (DA) pair recombination between an electron at the phosphorus donor and a hole at the zinc acceptor,



This conclusion is supported by several pieces of experimental evidence. First, in our study, as well as in the earlier studies,³⁻⁶ the antisite-related PL is only observed in p -type materials. Second, the strength of the PL increases as a function of the acceptor concentration. Finally, the shallow Zn acceptor resonance has recently been detected by ODMR in the 0.8–0.9-eV band by the application of uniaxial stress, directly confirming its role in the DA recombination process.¹³ For donor-acceptor pair recombination, the recombination energy ($h\nu_{\text{PL}}$) is given by

$$h\nu_{\text{PL}} = E_g - (E_A + E_D) + \frac{ne^2}{\epsilon r} - E_{\text{rel}}, \quad (7)$$

where E_g is the band-gap energy, E_A and E_D are the ionization energies of the acceptor and the donor, respectively, ϵ is the static dielectric constant, ne the charge on the donor in the ground state, and r the separation of the donor and the acceptor. E_{rel} is the relaxation energy.

A characteristic feature of DA emission is a shift of the PL-ODMR band to higher energies with increasing modulation frequency of the microwaves because of the shorter radiative lifetime of the close pairs (which have a larger Coulomb term $ne^2/\epsilon r$). In the case of the A band, this feature is demonstrated in Fig. 10. In Figs. 10(a) and 10(b), the peak of luminescence shows a ~ 0.05 -eV shift vs the modulation frequency. A comparison of Figs. 10(a) and 10(b) reveals a similar shift vs excitation energy, as also expected for DA luminescence. The spectra taken at 1.1-KHz modulation frequency and the higher excitation energy reflect the close donor-acceptor pairs, whereas the spectra taken at 12-Hz modulation frequency and the lower excitation energy reflect the more distant donor-acceptor pairs.

Figure 11 represents a combination of the ODMR emission and excitation spectral dependences of the isolated antisite A band in sample no. 2. In the figure, (I) duplicates the emission spectral dependence of ODMR spectrum A shown in Fig. 10, and (II) duplicates its excitation spectral dependence shown in Fig. 9. The solid curves, taken at 1.1 KHz, reflect the close donor-acceptor pairs. The dashed curves, taken at 12 Hz, reflect the more distant donor-acceptor pairs. We see that for the

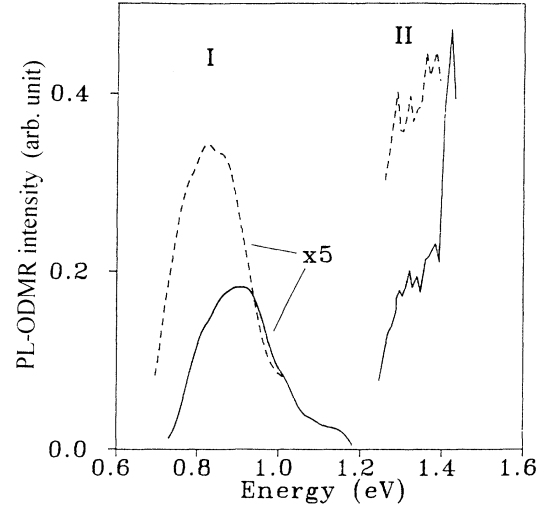


FIG. 11. Emission (I) and excitation (II) spectra, summarized from Figs. 9 and 10, for the A -band PL-ODMR in sample no. 2. The solid lines taken at 1.1-KHz modulation (and 1.39-eV excitation for the emission spectrum) reflect the closer donor-acceptor pairs. The dashed lines, taken at 12-Hz modulation (and 1.34-eV excitation), reflect the more distant pairs.

close pairs the high-energy detection limit of the PL-ODMR signal almost coincides with the low-energy limit of the excitation spectrum at about 1.2 eV. For the distant DA pair, the limit is shifted to ~ 1.1 eV.

We use Eq. (7) to estimate the energy positions of the $P_{\text{In}}^+/P_{\text{In}}^{2+}$ level. We insert $n = 2$, and, with the binding energy, ~ 46 meV of the Zn acceptor, Eq. (7) simplifies to

$$h\nu_{\text{PL}} \cong E(P_{\text{In}}^{+/2+}) + \frac{2e^2}{\epsilon r} - E_{\text{rel}} - 0.046 \text{ eV}, \quad (8)$$

where $E(P_{\text{In}}^{+/2+})$ is measured from the valence band edge. At a Zn doping level of $\sim 10^{16}$ (sample no. 2), a maximum average distant DA pair separation can be estimated to be $\sim \frac{1}{2}(10^{24}/10^{16})^{1/3} \sim 200$ Å. For this separation, the Coulomb term $2e^2/\epsilon r \sim 0.01$ eV is negligible and can be ignored for the distant pairs. For the excitation, the direct acceptor-to-donor transitions are probably weak, the spectral dependence obtained reflecting primarily transitions from the high density of states at the top of the valence band. For this, therefore, the acceptor level position is not involved, and

$$h\nu_{\text{exc}} \cong E(P_{\text{In}}^{+/2+}) + \frac{2e^2}{\epsilon r} - E_{\text{rel}}. \quad (9)$$

For both luminescence and excitation, the onset is given by $E_{\text{rel}} = 0$ (zero phonon transition). With Eqs. (8) and (9), the average onset deduced from comparison of the excitation and luminescence spectra becomes

$$h\nu_{\text{onset}} \cong E(P_{\text{In}}^{+/2+}) + \left\langle \frac{2e^2}{\epsilon r} \right\rangle - 0.023 \text{ eV}. \quad (10)$$

Ignoring the last two terms which are small and partially canceling, the 1.1-eV onset deduced for the distant pairs leads to an estimate for the isolated $P_{\text{In}}^{+/2+}$ level posi-

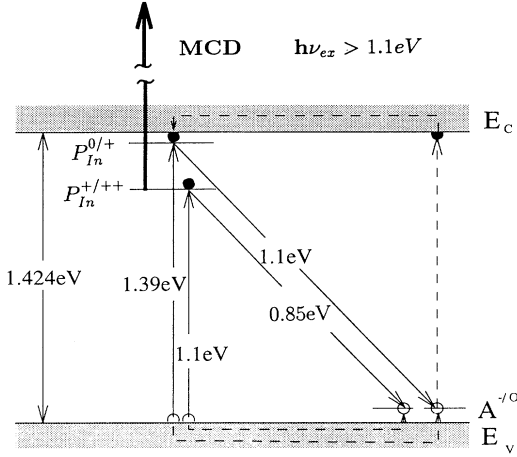
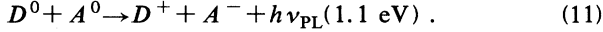


FIG. 12. Level structure deduced for the isolated P_{In} antisite. The energies indicated for the excitation thresholds (vertical arrows) give the level positions. The energies indicated for the luminescence transitions are for the maximum of each transition, and therefore differ due to lattice relaxations (Stokes shifts).

tion of $E_V + 1.1 \pm 0.1$ eV. The peak of the luminescence band at 0.85 eV reveals an average $E_{rel} \sim 0.25$ eV in the transition. This energy, which is the difference in the relaxation energies between the excited P_{In}^+ and ground P_{In}^{2+} states, is close to that estimated in the similar case of isolated P_{Ga} in GaP (Ref. 14) and therefore appears reasonable. These results are summarized in the energy level diagram of Fig. 12.

2. B band

ODMR spectrum *B* arises from an efficient recombination process that is in competition with the *A* luminescence. This suggests for the *B* luminescence DA pair recombination with another donor state, higher in the band gap than the P_{In}^+/P_{In}^{2+} level,

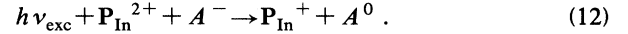


This donor could be unrelated to the antisite, the competition arising from the limited number of A^0 states with which the two donors (D^0 and P_{In}^+) can recombine. However, this does not explain easily why the negative P_{In}^+ ODMR signal seen in the 1.1-eV luminescence arises from the isolated antisites with very long lifetimes (far removed from acceptors), as concluded in Sec. IV. On the other hand, it can be explained easily if the D^0 state is isolated P_{In}^0 . In this case, the sharp excitation onset at 1.39 eV corresponds to the excitation of an electron from the valence band to the $P_{In}^{0/+}$ level, as shown in Fig. 12. For this to occur, the antisite must already have been excited into the P_{In}^+ state and have a long enough lifetime for the second excitation, thus favoring those far removed from acceptors. ODMR transitions at these P_{In}^+ states increase the *A*-band luminescence, but decrease the *B*-band luminescence by decreasing the

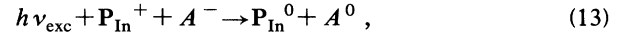
steady-state concentration of P_{In}^+ states for the *B*-band excitation. Since the excitation is at the antisite far from acceptors, no Coulomb correction is needed and the $P_{In}^{0/+}$ level position is estimated to be $E_V + 1.39 \pm 0.03$ eV. The peak of the luminescence at 1.1 eV implies again a lattice relaxation of ~ 0.03 eV for this transition also. (Such a large relaxation energy is not normally expected for a shallow donor state. If our interpretation is correct, the P_{In}^0 state must therefore be shallow only in the electrical sense and deep as regards its electron localization and accompanying lattice relaxation.) These results are also indicated in Fig. 12.

We note that the 1.39-eV excitation threshold might alternatively be assigned to the acceptor ($E_V + 0.046$ eV) to conduction-band transition, the electron produced subsequently being trapped at the $P_{In}^{0/+}$ level. To account for this possibility, which would imply a somewhat shallower $P_{In}^{0/+}$ level but still in the band gap, we place the ± 0.03 -eV uncertainty estimate on its level position.

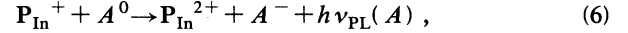
Here we summarize our model. There are a fixed number of isolated antisite defects, each of which exists in one of three possible charge states at any one time: P_{In}^0 , P_{In}^+ , and P_{In}^{2+} . In *p*-type material, P_{In}^{2+} is the stable state before excitation. For photoexcitation $h\nu > 1.1$ eV, P_{In}^+ is generated by



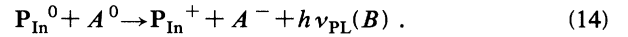
For photoexcitation $h\nu > 1.39$ eV,



generating the P_{In}^0 state. The reverse recombination processes produce luminescence *A*



and *B*:



ODMR transitions for P_{In}^+ enhance Eq. (6), decreasing the concentration of P_{In}^+ and hence the generation of P_{In}^0 via Eq. (13). The subsequent *B* luminescence via Eq. (14) therefore decreases. The *B* luminescence comes primarily from antisites far removed from acceptors which have the longer lifetimes for their photogenerated P_{In}^+ states. As a result, the negative P_{In}^+ ODMR signal observed in the *B* luminescence is seen at low modulation frequencies and displays broader lines, the P_{In}^+ lifetime becoming comparable to nuclear relaxation times.

B. P_{In}^+ MCD in *p*-type material

The isolated antisite is observed via PL-ODMR and PL-ODENDOR in the as-grown sample no. 2. At the same time, the isolated antisite is detected via MCD-ODMR and MCD-ODENDOR in the same sample. This unexpected result was pointed out by us in an earlier study,¹⁵ before we were aware of the significance of the *B* band and its negative ODMR signals. It was not expected for the following reasons: Optical detection of magnetic resonance is possible when the intensity of a

transition can be affected by changing the spin of a paramagnetic initial state. Optical absorption usually takes place from a stable ground state of a defect, whereas emission is from an excited state to the ground state. Therefore the same paramagnetic state cannot be an initial state in both absorption and emission unless it is an excited state from which both radiative recombination and absorption can take place.

We illustrate this with the optical transitions involving the P_{In}^+ state of the isolated antisite defect. The MCD-ODMR signal is detected as a resonant decrease of the difference between optical absorption of right and left circularly polarized light in the following transition from the paramagnetic P_{In}^+ state:



where $(P_{\text{In}}^+)^*$ is an excited state of P_{In}^+ . Obviously this transition is expected to be strong when P_{In}^+ is the stable state in thermal equilibrium but weak or absent when the diamagnetic P_{In}^{2+} state is the stable one. The PL-ODMR signal, on the other hand, is detected as a resonant change in the intensity of a radiative recombination from the paramagnetic P_{In}^+ state. For donor-to-acceptor recombination in p -type material, P_{In}^{2+} is the stable state and the A luminescence arises from radiative return of the hole to the excited P_{In}^+ state, described by Eq. (6).

Therefore we argued that the only way that the isolated antisite defect could reveal its P_{In}^+ paramagnetic charge state in both absorption and luminescence in the same p -type sample would be via a two-step excitation.¹⁵ If, for example, as illustrated in Fig. 12, light with energy corresponding to the absorption cross section of the MCD band in the band gap were capable of ionizing the diamagnetic P_{In}^{2+} state of the isolated antisite to the paramagnetic P_{In}^+ state as in Eq. (12), one could then also measure MCD via Eq. (15) provided that the photoexcited P_{In}^+ state has a long enough lifetime. The lifetime of P_{In}^+ depends on the concentration and distribution of acceptors to which radiative recombination from this state can take place according to Eq. (6). This recombination is fast for close P_{In}^+ acceptor pairs, explaining why we do not observe MCD adsorption in more heavily doped samples except when electron irradiated.

We now know that this is correct. The A -band PL excitation studies in Fig. 9(b) establish the threshold at ~ 1.1 eV for the isolated antisite, and therefore the higher energy 900–1000-nm light used for the MCD studies does indeed generate P_{In}^+ according to Eq. (12). That there are distant P_{In} -acceptor pairs of sufficiently long lifetime to generate a steady-state population of P_{In}^+ under excitation is therefore confirmed both by the MCD experiments and the negative B -line ODMR signals, which together provide additional confirmation of our P_{In}^0 interpretation of the B luminescence.

[The fact that P_{In}^+ is seen in MCD via a two-state process in p -type material can also supply an explanation for why the spectral dependence of the isolated P_{In}^+ MCD-ODMR of electron-irradiated sample no. 3C in Fig. 3 (curve c) appears to be shifted to lower energy than in the as-grown more lightly doped material. Electron ir-

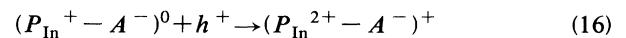
radiation produces strong absorption near the band edge, which reduces strongly the excitation intensity in this spectral region which is essential to generate the P_{In}^+ state in this heavily doped material, presumably still p type.]

We conclude, therefore, that the 900–1000-nm light used in the MCD studies (see Fig. 3) does indeed serve to photoionize P_{In}^{2+} of the isolated antisite in the p -type material, producing the P_{In}^+ and its MCD adsorption via a two-step process. Hence the fact that the MCD-ODMR signal is observed in p -type InP does not contradict its detection in the PL bands.

C. Model for the perturbed antisites

The level positions of the $P_{\text{In}}X$ and $P_{\text{In}}Y$ antisite defects cannot be determined from the present data. However, there are a few indications in the data which suggest that the $P_{\text{In}}^+/P_{\text{In}}^{2+}$ level of the perturbed antisites is higher in the band gap than the corresponding level of the isolated antisite. First, the ODMR signals of these antisite defects are only observed in originally n -type samples, or ones that have been electron irradiated to become n type. Second, the perturbed antisites seem to be shallower than the isolated one, as judged from the hyperfine interaction of the bound electron in the nearest-neighbor shells (Table III). The central hyperfine interaction on the P_{In} core is smaller for the combined perturbed antisites, $940 \times 10^{-4} \text{ cm}^{-1}$ instead of $980 \times 10^{-4} \text{ cm}^{-1}$ for the isolated one. A corresponding increase is observed in the ligand high-frequency (hf) interaction with the nearest-neighbor P and In shells. The hyperfine coupling constant A_{In} is 26% larger for the perturbed defects than for the isolated one, and the corresponding increase we have estimated for the four P neighbors is 25%. This extension of the electron wave function from the central P_{In} to its neighbors is consistent with a corresponding reduction in the electron binding energy.

From the experimental data a logical model for this antisite structure seems to be a PP_4 configuration with a disturbed nearest-neighbor In shell. A substitutional acceptor in the In shell agrees with most of our observations. For example, a close $P_{\text{In}}-A_{\text{In}}$ pair is likely to be a fast recombination center from which a two-step excitation is unlikely. Indeed, we never see MCD signals from this center unless the material is n type. The lifetime of the photoexcited $(P_{\text{In}}^+-A^-)^0$ paramagnetic state in p -type material can be expected to be short and dominated by the reverse hole recombination process



because, in contrast to the P_{In}^+ state of the isolated antisite, which repels the photoexcited hole, the hole is not repelled from the $(P_{\text{In}}^+-A^-)^0$ state. Accordingly, it should have a shorter lifetime than the paramagnetic state of the isolated antisite. Photoexcitation is therefore unlikely to build up enough population of the $(P_{\text{In}}^+-A^-)^0$ state that two-step MCD absorption can take place in p -type material. In n -type material, however, the neutral state is the stable state.

Also, a negatively charged acceptor A^- in the nearest-neighbor In shell will raise the $P_{\text{In}}^+/P_{\text{In}}^{2+}$ level position significantly compared to that of the isolated antisite. The Coulomb repulsion $e^2/\epsilon r$ from the negative acceptor experienced by a bound electron can be estimated to be ~ 300 meV for the P_{In}^-A distance 0.36 nm. Such an upward shift would be expected therefore for the levels of a P_{In}^-A defect, in which case its $(P_{\text{In}}^+ - A^-)^0 / (P_{\text{In}}^{2+} - A^-)^+$ level could be quite close to the conduction-band edge.

Our earlier studies¹⁰ in different n -type starting materials have provided strong evidence that the perturbed antisite defects are not present initially in the materials but are being produced by the irradiation. This suggests that the acceptor may be an In vacancy in the second neighbor shell.

VI. SUMMARY

In the present study we have measured a large number of InP samples representing different combinations of n - and p -type shallow doping and irradiation doses. The results are summarized in Table II. We have observed more than one antisite structure in InP, one of them being the isolated P_{In} antisite. The others are unidentified antisite defects characterized in ODENDOR measurements by a distortion in a near-neighbor shell.

ODENDOR signals of the isolated antisite have been found alone in the as-grown lightly doped p -type sample no. 2 via both PL and MCD, and also in the more heavily doped p -type starting material no. 3 via PL-ODENDOR for the as-grown material, and MCD-ODENDOR after electron irradiation. They are also observed weakly in electron-irradiated n -type starting material together with signals from the perturbed antisites. The MCD-ODMR values characteristic of samples which show only the ODENDOR spectrum of the isolated antisite are $g = 2.000 \pm 0.003$, and $A_0 = (980 \pm 30) \times 10^{-4} \text{ cm}^{-1}$ with a half-width of 350 ± 30 G for each of the two central phosphorus hf lines.

The perturbed antisites dominate the MCD-ODMR and MCD-ODENDOR in electron-irradiated n -type InP, but have also been observed with similar intensity in moderately doped p -type or semi-insulating starting material that has been converted to n type by electron irradiation. The values characteristic of samples which show only the MCD-ODENDOR spectrum of the perturbed antisite are $g = 1.990 \pm 0.005$, and $A_0 = (940 \pm 30) \times 10^{-4} \text{ cm}^{-1}$ with a half-width of 410 ± 30 G. As illustrated in Table II, some samples show all of the antisite signals simultaneously in ODENDOR. This situation is also reflected in the g and A_0 values, which tend to be a mixture of the above extreme values and consequently fail to tell unambiguously which antisite defect is present. We see for example that the ODMR signals in Fig. 1 are rather similar, although the differences in the corresponding ODENDOR signals in Fig. 2 which were measured in the same samples are quite apparent.

Photoluminescence in as-grown p -type InP materials reveals two ODMR bands, peaking at 0.8–0.9 and 1.1 eV. Our studies show that these two bands arise from two competitive recombination processes, one, labeled A , giving rise to a positive ODMR antisite signal, the other, labeled B , giving rise to a negative ODMR antisite signal. ODENDOR studies reveal that both ODMR spectrum A and B arise from the isolated antisite. We proposed that band A arises from donor-acceptor recombination involving P_{In}^+ and band B arises from similar recombination involving P_{In}^0 , which is generated by a second hole ionization excitation from P_{In}^+ . This occurs primarily at antisites far removed from acceptors where the photogenerated P_{In}^+ state has a sufficiently long lifetime for the second excitation to occur. Evidence cited for this is the dominance of spectrum B at low modulation frequencies, and a broader flat-topped linewidth, indicating that the lifetime has become comparable to nuclear relaxation times. Studies of the PL-ODMR excitation and emission spectra and their dependence upon modulation frequency has allowed us to estimate the level positions for the isolated antisite. They are $E_V + 1.1 \pm 0.1$ eV for the $P_{\text{In}}^+/P_{\text{In}}^{2+}$ level, and $E_V + 1.39 \pm 0.03$ eV for the $P_{\text{In}}^0/P_{\text{In}}^+$ level.

This same two-step excitation allows MCD detection of P_{In}^+ of the isolated antisite in as-grown lightly doped p -type material, even though the $P_{\text{In}}^+/P_{\text{In}}^{2+}$ level is more than 1.1 eV above the valence-band edge. In as-grown more heavily doped p -type material, isolated antisite MCD signals are not observed. This is presumably due to the fact that the shallow acceptors provide fast radiative recombination channels, and the lifetime of photogenerated P_{In}^+ is too short. Electron irradiation is likely to passivate these channels which can make the P_{In}^+ state of the isolated antisite observable via MCD either directly, if the charge state is right, or via two-step excitation. The fact that the irradiation quenches the radiative recombination between the P_{In}^+ state and the acceptors supports this hypothesis.

At least two distinct perturbed antisites, labeled $P_{\text{In}}(X)$ and $P_{\text{In}}(Y)$, have been detected via MCD-ODENDOR in electron-irradiated n -type material. Previous studies have concluded that they are not initially present in the as-grown material but are produced by the irradiation. Analysis of their ODMR linewidth and the fact that they are only seen in n -type material indicates that their electrical levels are higher in the gap than those of the isolated antisite. This suggests that the nearby perturbing defect X or Y is an acceptor. A possible candidate is an indium vacancy in the nearest In neighbor shell.

ACKNOWLEDGMENTS

This research has been supported by the National Science Foundation under Grant Nos. DMR-89-02572 and DMR-92-04114. The participation of H.P.G. was supported by NATO Scientific Affairs Division under Grant No. 0499/87 and the Icelandic Council of Science.

- *Permanent address: Science Institute, University of Iceland, Dunhaga 3, 107 Reykjavik, Iceland.
- †Permanent address: Army Research Laboratory, EPSC, AMSRL-EP-EC Fort Monmouth, NJ 07703.
- ¹T. A. Kennedy and N. D. Wilsey, *Appl. Phys. Lett.* **44**, 1089 (1984).
- ²M. Deiri, A. Kana'ah, B. C. Cavenett, T. A. Kennedy, and N. D. Wilsey, *J. Phys. C* **17**, L793 (1984).
- ³L. H. Robins, P. C. Taylor, and T. A. Kennedy, *Phys. Rev. B* **38**, 13 227 (1988).
- ⁴B. C. Cavenett, A. Kana'ah, M. Deiri, T. A. Kennedy, and N. D. Wilsey, *J. Phys. C* **18**, L473 (1985).
- ⁵T. A. Kennedy and N. D. Wilsey, *J. Cryst. Growth* **83**, 198 (1987).
- ⁶M. Deiri, A. Kana'ah, B. C. Cavenett, T. A. Kennedy, and N. D. Wilsey, *Semicond. Sci. Technol.* **3**, 706 (1988).
- ⁷A. Kana'ah, M. Deiri, B. C. Cavenett, N. D. Wilsey, and T. A. Kennedy, *J. Phys. C* **18**, L619 (1985).
- ⁸D. Y. Jeon, H. P. Gislason, J. F. Donegan, and G. D. Watkins, *Phys. Rev. B* **36**, 1324 (1987).
- ⁹K. Ando, A. Katsui, D. Y. Jeon, G. D. Watkins, and H. P. Gislason, *Mater. Sci. Forum* **38-41**, 761 (1989).
- ¹⁰H. P. Gislason, H. J. Sun, R. Peale, and G. D. Watkins, *Mater. Sci. Forum* **83-87**, 905 (1992).
- ¹¹H. C. Crookham, T. A. Kennedy, and D. C. Treacy, *Phys. Rev. B* **46**, 1377 (1992).
- ¹²W. A. Barry, Ph.D. dissertation, Lehigh University, 1992 (unpublished).
- ¹³T. A. Kennedy, H. C. Crookham, E. R. Glaser, and R. L. Henry, *Bull. Am. Phys. Soc. B* **38**, 266 (1993).
- ¹⁴K. P. O'Donnell, K. M. Lee, and G. D. Watkins, *Solid State Commun.* **44**, 1015 (1982).
- ¹⁵H. P. Gislason, H. Sun, F. Rong, and G. D. Watkins, in *The Physics of Semiconductors*, edited by E. M. Anastassakis and J. D. Joannopoulos (World Scientific, Singapore, 1990), p. 660.